Inorganic Chemistry

Article

pubs.acs.org/IC

Electronic Properties of [Core+*exo*]-type Gold Clusters: Factors Affecting the Unique Optical Transitions

Yukatsu Shichibu and Katsuaki Konishi*

Faculty of Environmental Earth Science, Hokkaido University, North 10 West 5, Sapporo 060-0810, Japan

Supporting Information

ABSTRACT: Unusual visible absorption properties of [core+*exo*]-type Au_6 (**1**), Au_8 (**2**), and Au_{11} (**3**) clusters were studied from experimental and theoretical aspects, based on previously determined crystal structures. Unlike conventional core-only clusters having no *exo* gold atoms, these nonspherical clusters all showed an isolated visible absorption band in solution. Density functional theory (DFT) studies on corresponding nonphenyl models (**1′**−**3′**) revealed that they had similar electronic structures with discrete highest occupied molecular orbital (HOMO) and lowest unoccupied molecular orbital (LUMO) bands. The theoretical spectra generated by time-dependent DFT (TD-DFT) calculations agreed well with the experimentally measured properties of **1**−**3**, allowing assignment of the characteristic visible bands to HOMO−LUMO transitions. The calculated HOMO−LUMO transition energies increased in the order Au_{11} < Au_6 < Au_8, as was found experimentally. Frontier orbital analyses indicated that the HOMO and LUMO were both found in proximity to the terminal Au_3 triangles containing the *exo* gold atom, with the HOMO → LUMO transition occurring in the core → *exo* direction. The HOMO/LUMO distribution patterns of **1′** and **3′** were similar to each other but were markedly different from that of **2′**, which has longer core-to-*exo* distances. These findings showed that not only nuclearity (size) but also geometric structures have profound effects on electronic properties and optical transitions of the [core+*exo*]-type clusters.

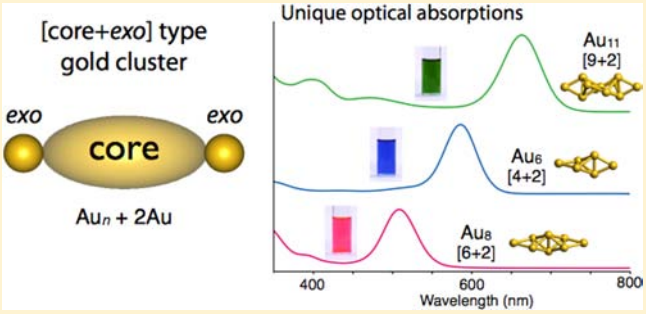

INTRODUCTION

Metal nanoparticles and clusters have attracted continuing attention from both practical and fundamental aspects in relation to their unique optical, electronic, and catalytic properties.[1−4] The most prominent property of metal nanoparticles with sizes of ∼2 nm or above is localized surface plasmon bands, which have been widely exploited for biomedical applications.[5,6] However, when the object's size approaches the Fermi wavelength of electrons, such plasmon resonances disappear and discrete electronic transitions emerge instead.[7−9] Such molecule-like features are observed for small clusters with nuclearity less than ∼40, which exhibit structured visible absorptions. Furthermore, some subnanometer-sized clusters with a nuclearity of around 10 have been reported to be photoluminescent, attracting special attention in relation to the development of fluorescent probes.[10−14] In such small clusters, not only the nuclearity but also the geometric structure should noticeably affect their electronic structures. However, the origin and nature of their optical properties has not been fully clarified because of the lack of structural information.

Single-crystal X-ray analyses provide precise structural information, thus being most useful for elucidating the relationship between the geometry and the optical properties of ultrasmall molecular clusters. The molecular structures of numerous phosphine- and thiolate-coordinated gold clusters with well-defined nuclearity, which form major families in cluster chemistry, have been reported.[15−32] From a structural standpoint, phosphine-coordinated clusters can be simply partitioned into the inorganic moiety (metal) and surrounding organic ligands (shell) because of the neutral character of phosphine, whereas thiolate-capped clusters are rather complicated because the gold core is covered by a gold−thiolate layer.[30−32] Thus, the phosphine-coordinated family offers suitable structural models for studying the nature of the central gold moieties. The crystal structures of monophosphine-coordinated clusters (Au_7,[19] Au_8,[20] Au_9,[21] Au_{11},[22−24] Au_{13}[25,26]) have indicated that the gold units favor icosahedron-based geometries. However, some exceptional nonspherical structures have also been known to form when chelating diphosphines were utilized as the protecting ligands. An example is the [core+*exo*]-type cluster bearing extra gold atoms attached to a polyhedron-based core, first reported by van der Velden et al. for the Au_6 cluster $[Au_6(dppp)_4]^{2+}$ (**1**) (dppp = $Ph_2P(CH_2)_3PPh_2$) with a tetrahedral Au_4 core and two gold atoms at the *exo* positions (Figure 1).[27] We have recently synthesized a higher nuclearity series with similar structural features ($[Au_8(dppp)_4Cl_2]^{2+}$ (**2**)[28] and $[Au_{11}(dppe)_6]^{3+}$ (**3**)[29] (dppe = $Ph_2P(CH_2)_2PPh_2$)), whose structures were established by X-ray crystallography. One of the notable common features

Received: March 5, 2013
Published: May 16, 2013

   dx.doi.org/10.1021/ic4005592 | *Inorg. Chem.* 2013, 52, 6570−6575

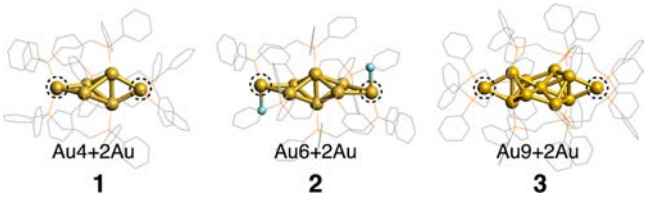

Figure 1. Crystal structures of Au_n + 2Au ([core+*exo*] type) clusters $[Au_6(Ph_2P(CH_2)_3PPh_2)_4]^{2+}$ (**1**), $[Au_8(Ph_2P(CH_2)_3PPh_2)_4Cl_2]^{2+}$ (**2**), and $[Au_{11}(Ph_2P(CH_2)_2\ PPh_2)_6]^{3+}$ (**3**). *Exo* gold atoms are highlighted by dotted circles.

of these clusters is their unusual optical properties, which are substantially different from those of conventional sphere-like gold clusters. In a preliminary communication, we have reported a clear example of shape-dependence in the optical properties of **3** and the isomeric spherical Au_{11} cluster ($[Au_{11}(dppp)_5]^{3+}$).[29]

In the present paper, we report the results of systematic studies on the optical properties of the above three [core+*exo*] type clusters (**1**−**3**) possessing different nuclearity based on the known geometric structures.[27−29] In the nanosize regime, metal atom assemblies show size-dependent properties, generally known as quantum size effects.[7] Typically, the lowest optical transition energy increases as the size of the assembled object is reduced. However, little is known about the lower limit of this rule. Recently, density functional theory (DFT) calculations have been widely utilized as a powerful tool to investigate the geometric and electronic structures as well as the optical properties of small metal clusters.[32−36] Here we have investigated the electronic properties of the [core+*exo*]-type Au_6, Au_8 and Au_{11} clusters (**1**−**3**) using experimental and theoretical methods to identify the factors governing their unique electronic properties. We show that the electronic structures and optical properties of the [core+*exo*]-type clusters depend critically not only on the size (nuclearity) of the cluster unit, but also the geometric structure.

RESULTS AND DISCUSSION

Geometric Structures. The crystal structures of $[Au_6(dppp)_4]^{2+}$ (**1**), $[Au_8(dppp)_4Cl_2]^{2+}$ (**2**), and $[Au_{11}(dppe)_6]^{3+}$ (**3**) shown in Figure 1 reveal two gold atoms attached at the *exo* positions of each Au_n core, thus being depicted as core+two (Au_n + 2Au)-type clusters.[27−29] Each *exo* gold atom of **1** and **3** accommodates two phosphorus atoms from the neutral phosphine ligands, while those of **2** each accommodate one phosphorus atom from a phosphine and one anionic chloride ligand. The Au−Au bond distances in the polyhedral core units of all clusters were in the range 2.629−2.971 Å, similar to values reported for conventional spherical-type clusters such as $[Au_{13}P_{10}Cl_2]^{3+}$ (P: phosphine ligand) (2.696−2.974 Å).[25,26] The Au−Au bond distances involving the *exo* gold atoms of **1** and **3** (2.798 and 2.777−2.824 Å, respectively) were comparable to those observed in the core units, but were markedly shorter than those of **2** (2.970−3.072 Å). The long *exo*-to-core distance in **2** was attributed to the electron-withdrawing character of the anionic ligands (Cl^-) attached to the *exo* gold atoms, which may weaken the Au−Au interaction between the *exo* Au atoms and the central Au_6 unit.

Experimental Absorption Spectra. Solutions of the crystallized samples of **1**·$(NO_3)_2$, **2**·$(PF_6)_2$, and **3**·$(SbF_6)_3$ in dichloromethane were deeply colored, and were considerably different from each other (Figure 2A, pictures). Their

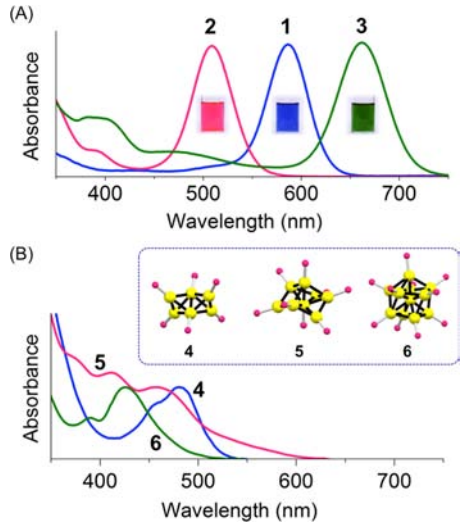

Figure 2. Solution absorption spectra of (A) [core+*exo*]-type (Au_n + 2Au) clusters $[Au_6(Ph_2P(CH_2)_3PPh_2)_4](NO_3)_2$ (**1**·$(NO_3)_2$), $[Au_8(Ph_2P(CH_2)_3PPh_2)_4Cl_2](PF_6)_2$ (**2**·$(PF_6)_2$), and $[Au_{11}(Ph_2P(CH_2)_2PPh_2)_6](SbF_6)_3$ (**3**·$(SbF_6)_3$), and of (B) core-only type isomers $[Au_6(PPh_3)_6](NO_3)_2$ (**4**·$(NO_3)_2$), $[Au_8(PPh_3)_8](BF_4)_2$ (**5**·$(BF_4)_2$), and $[Au_{11}(PMe_2Ph)_{10}](BPh_4)_2$ (**6**·$(BPh_4)_2$). Solvent: dichloromethane for **1**−**4** and **6**; methanol for **5**. Pictures of the solution samples of **1**−**3** and X-ray-based geometric structures of **4**−**6** (shown only for the Au and P atoms) are also provided in (A) and (B), respectively. The structures and spectra of **4**−**6** were taken from the papers by Mingos et al. (refs 15 and 18).

absorption spectra all showed an intense band in the visible region, fairly well-separated from the weak short-wavelength bands spreading into the UV region (Figure 2A). The spectra in acetonitrile or methanol were almost identical to those observed in dichloromethane (Supporting Information, Figure S1). Further, no substantial differences were observed between the spectra of **2**·Cl_2, **2**·$(SbF_6)_2$, and **2**·$(PF_6)_2$ (Supporting Information, Figure S1b). Therefore, the observed absorption spectra appeared to originate virtually from the cationic cluster moiety.

It should be noted that the spectral feature observed for the core+*exo* clusters (**1**−**3**) were distinctly different from those reported for conventional core-only type clusters. Mingos et al. reported the spectra of the core-only isomers with the same nuclearity ($[Au_6(PPh_3)_6](NO_3)_2$ (**4**·$(NO_3)_2$),[18] $[Au_8(PPh_3)_8](BF_4)_2$ (**5**·$(BF_4)_2$),[20] and $[Au_{11}(PMe_2Ph)_{10}](BPh_4)_3$ (**6**·$(BPh_4)_3$)[22]), which all display bands in the visible region, but they are obviously overlapped with the higher energy bands and the broad tailing from the UV region (Figure 2B).[15] Therefore, the "isolated" absorption bands were likely a common feature of [core+*exo*] type clusters. The *exo* gold atoms appeared to play a crucial role in the generation of unique electronic structures, since the attachment of extra gold atoms to the polyhedral core dramatically altered the absorption spectra. Actually, the core-only type Au_6 cluster (**4**), which had the same bitetrahedral geometry as the core of the Au_6+2Au-type Au_8 cluster (**2**), exhibited a spectral profile markedly different from that of **2** (Figure 2).

The observed intense absorption bands of **1**−**3** appeared to be the lowest energy excitations since no absorptions were found in the near-IR region. It should also be noted that they all presented similar symmetrical shapes (Figure 2A), suggesting that they all arose from single electronic transitions despite

dx.doi.org/10.1021/ic4005592 | *Inorg. Chem.* 2013, 52, 6570−6575

Table 1. Solution Absorption Spectral Data of 1−6[a]

entry	cluster	nuclearity	structure type	solvent	band wavelength [nm][d]	lowest-energy band	
						energy [eV]	ε [M^{-1} cm^{-1}]
1[b]	**1**·$(NO_3)_2$	6	Au_4+2Au	CH_2Cl_2	587 (1.00), 432 (0.05), 326 (0.43)	2.11	8.9×10^4
2[b]	**2**·$(PF_6)_2$	8	Au_6+2Au	CH_2Cl_2	508 (1.00), 390 (0.25), 322 (1.78)	2.44	2.7×10^4
3[b]	**3**·$(SbF_6)_3$	11	Au_9+2Au	CH_2Cl_2	663 (1.00), 471 (0.19), 390 (0.44), 316 (1.00)	1.87	8.9×10^4
4[c]	**4**·$(NO_3)_2$	6	core-only	CH_2Cl_2	476 (1.00), 452 (0.78), 330 (4.29), 319 (4.50)	2.60	nd[e]
5[c]	**5**·$(BF_4)_2$	8	core-only	CH_2Cl_2	460 (1.00), 412 (1.21), 370 (1.41)	2.69	nd[e]
6[c]	**6**·$(BPh_4)_3$	11	core-only	CH_2Cl_2	422 (1.00), 374 (0.46)	2.94	2.2×10^4

[a]In 10-mm quartz cell at 25 °C. [b]This work. [c]From ref 15. [d]Shown for the bands at >300 nm. The numbers in parentheses are absorbances relative to the lowest-energy band. [e]Not shown in ref 15.

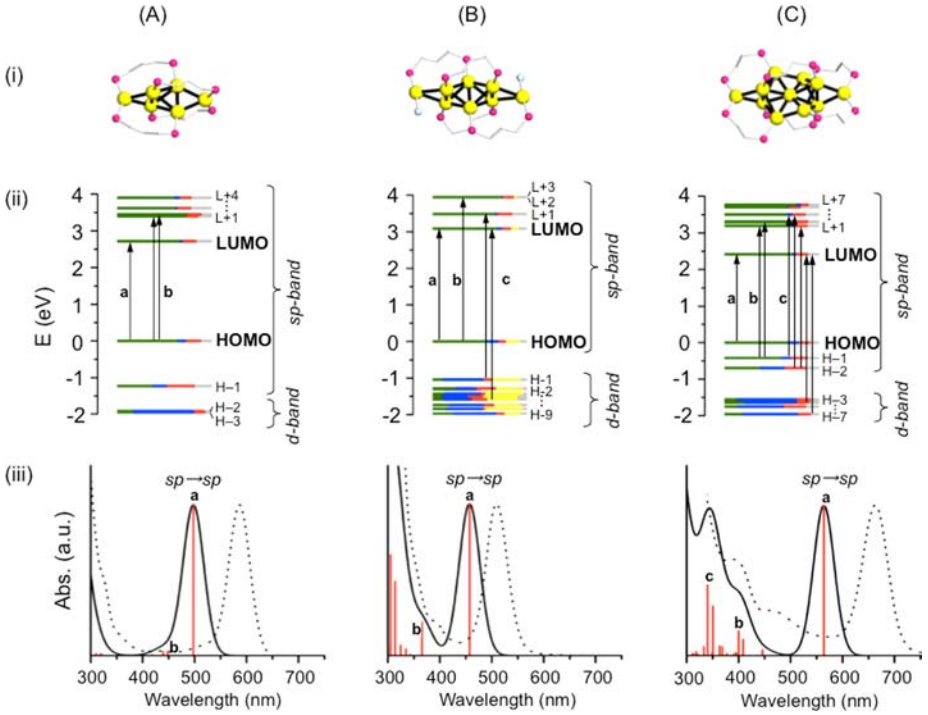

Figure 3. (i) Geometric structures of (A) $[Au_6(H_2P(CH_2)_3PH_2)_4]^{2+}$ (**1′**), (B) $[Au_8(H_2P(CH_2)_3PH_2)_4Cl_2]^{2+}$ (**2′**), and (C) $[Au_{11}(H_2P(CH_2)_2PH_2)_6]^{3+}$ (**3′**) with Au, P, and Cl atoms highlighted in yellow, magenta, and light blue, respectively, and H atoms omitted for clarity. (ii) Kohn−Sham (KS) orbital energy level diagrams. (iii) Theoretical absorption spectra (solid lines) and experimental spectra (dotted lines). Each KS orbital energy is relative to the HOMO energy and is drawn to indicate the relative contributions (line lengths with color labels) of the atomic orbitals of Au (6sp) in green, Au (5d) in blue, P (3p) in red, Cl (3p) in yellow, and others in gray.

their different transition energies. The observed band positions for **1**−**3** were at 587, 508, and 663 nm, respectively. That is, the first excitation energy increased in the order Au_{11} (**3**, 1.87 eV) < Au_6 (**1**, 2.11 eV) < Au_8 (**2**, 2.44 eV), not matching the order of nuclearity. Therefore, the optical properties of [core+*exo*] type clusters depended on geometry rather than size (nuclearity). Table 1 summarizes the optical absorption data of **1**−**3** and relevant core-only isomers (**4**−**6**), together with the molar extinction coefficients (ε) of **1**−**3**. The lowest-energy bands of the core-only clusters (**4**−**6**) were observed at definitely higher energies than those of the core+*exo* type clusters (**1**−**3**). The ε values of the all-phosphine type clusters (**1** and **3**) were similar to each other, but noticeably larger than that of **2** with the anionic coordinating ligands. **1** and **3** gave similar ε values (8.9×10^4), which was roughly three times larger than that of **2** (2.7×10^4).

Electronic Structures. The above-mentioned experimental data clearly demonstrated that the electronic structures of these clusters depend more strongly on geometric structure than on nuclearity (size). To understand the relationship between geometric and electronic structure, we performed DFT calculations on nonphenyl models of **1**−**3**, namely, $[Au_6(H_2P(CH_2)_3PH_2)_4]^{2+}$ (**1′**), $[Au_8(H_2P(CH_2)_3PH_2)_4Cl_2]^{2+}$ (**2′**), and $[Au_{11}(H_2P(CH_2)_2PH_2)_6]^{3+}$ (**3′**). Kohn−Sham molecular orbitals (MOs) for the three clusters are shown in Figure 3 (ii), in which it can be seen that they showed similar distributions, with the highest occupied molecular orbitals (HOMOs) and lowest unoccupied molecular orbitals (LUMOs) appreciably separated from their closest orbitals (HOMO−1 and LUMO+1, respectively). The atomic orbital contributions revealed that unoccupied orbitals, the HOMO, and certain high-energy occupied orbitals (HOMO−1 for **1′** and HOMO−1 and −2 for **3′**) were predominantly constituted by Au(6sp) atomic orbitals, thus forming sp-bands. The contributions from P (3p, red) and Cl (3p, yellow) of the coordinating ligands were not significant (less than ∼20%). On the other hand, the lower-energy occupied molecular orbitals were predominantly composed of the 5d atomic orbitals of gold (blue), constituting d-bands.

dx.doi.org/10.1021/ic4005592 | *Inorg. Chem.* 2013, 52, 6570−6575

Charge Distribution Analysis. The three core+*exo* clusters are positively charged (2+ for **1′** and **2′**, 3+ for **3′**), so the cluster units contain formally zerovalent and ionic (Au^+, Au^{3+}) gold atoms. Therefore it should be of interest to investigate the distribution of charge on the constituent atoms. In this context, a recent theoretical study of a spherical phosphine/chloride-coordinated Au_{11} cluster (**6′**, $Au_{11}(PH_3)_7Cl_3$) demonstrated that the gold core and chloride ligands were negatively charged (Table 2, entry 4), compensated for by positively charged phosphine ligands.[34] Charge distribution profiles of **1′**−**3′** based on a simple Mulliken population analysis (entries 1−3) showed similar trends, giving negative charges on the gold cluster units and positive charges on the phosphine ligands. However, among individual gold atoms in a cluster, the *exo* gold atoms were clearly positively charged (+0.3 to +0.4 for each atom), whereas the polyhedral core units were negatively charged. This trend agreed with that expected from the Mingos' capping principle.[37] Also of note was the fact that the *exo* gold atoms of **2′**, bonded to electron-withdrawing Cl, carried similar positive charges (entry 2) to those of the phosphine-only clusters (**1′** and **3′**, entries 1 and 3). Therefore, the effect of the nature of coordinating ligands on the ionic character of the *exo* gold atoms is not so significant, while it definitely affected the core-to-*exo* distances as found in the geometric structures.

Table 2. Calculated Charges for the Components of 1′−3′ and 6′

entry	cluster	total charge	core Au	exo Au	phosphine	Cl
1	**1′**[a]	2+	−1.15	+0.72	+2.43	
2	**2′**[a]	2+	−0.79	+0.60	+2.62	−0.43
3	**3′**[a]	3+	−1.38	+0.78	+3.62	
4	**6′**[b]	0	−0.77		+2.38	−1.61

[a]CAO-based Mulliken charges estimated by a program in TURBOMOLE package. [b]Ref 34.

Theoretical Absorption Spectra. We further performed time-dependent DFT (TD-DFT) calculations to simulate the absorption spectra of **1′**−**3′** and found that the theoretical results reproduce well the experimental observations (Figure 3 (iii)). For example, the lowest-energy excitation due to the HOMO → LUMO intraband (sp → sp) transition of **1′** was dominant in oscillator strength (a in Figure 3A (iii)) and separated from the other higher-energy transitions worthy of consideration (e.g., b in Figure 3A (iii)) (Table 3). Consequently, the HOMO → LUMO transition gave a single isolated band in the simulated spectrum, as was observed experimentally (Figure 3A (iii)). Analogous calculations on **2′** and **3′** gave HOMO → LUMO transitions with high oscillator strengths (a in Figure 3B and C (iii)), which were energetically separated from the other transitions (b, c) including interband d → sp transitions, thereby giving rise to isolated intense visible bands in the simulated spectra. Overall, the theoretical spectra of **1′**−**3′** agreed well with the experimental spectra, especially their spectral shapes, and so the experimentally observed intense absorption bands were all assigned to HOMO → LUMO electronic transitions. Considering the above-mentioned contributions of atomic orbitals to the HOMOs and LUMOs, the visible absorptions have little ligand-mediated character, but rather, were likely due to metal-centered or intermetal transitions. The calculated HOMO−LUMO transition energies, which correspond to the first excitation energies, increased in the order **3′** (Au_{11}, 2.20 eV) < **1′** (Au_6, 2.49 eV) < **2′** (Au_8, 2.71 eV). Although there was a discrepancy between the calculated and experimental energy values, which may be due to the effect of the phenyl groups attached to the P atoms[38] and TD-DFT errors, the order of the energies was consistent with those in the experiments, again indicating the absence of correlation between first excitation energy and nuclearity in these clusters.

Table 3. Optical Transitions of 1′−3′ Generated by TD-DFT Calculations[a]

	energy (eV)/wavelength (nm)	oscillator strength	assignment[b]
1′	2.49/498	0.5148	HOMO→LUMO (a)
	2.77/448	0.0151	HOMO→LUMO+1 (b)
	2.82/440	0.0138	HOMO→LUMO+2 (b)
2′	2.71/457	0.3433	HOMO→LUMO (a)
	3.39/366	0.0761	HOMO→LUMO+2 (b)
	3.95/314	0.1675	HOMO-1→LUMO+1 (c)
	4.06/305	0.2278	HOMO-6→LUMO (c)
3′	2.20/564	0.5917	HOMO→LUMO (a)
	3.03/409	0.0636	HOMO-1→LUMO+1 (b) HOMO-1→LUMO+2 (b)
	3.10/400	0.1382	HOMO-1→LUMO+2 (b) HOMO-1→LUMO+1 (b)
	3.54/350	0.1949	HOMO-1→LUMO+4 (c) HOMO-2→LUMO+1 (c)
	3.64/340	0.2844	HOMO-2→LUMO+4 (c)

[a]Only the transitions with relatively high oscillator strengths are shown. [b]a−c in parentheses correspond to the transitions given in Figure 3 (ii) and (iii).

Frontier Orbital Distribution. As noted above, the intense visible bands, which were unique to **1**−**3**, originate from the lowest energy HOMO → LUMO transitions. To obtain further insight into the nature of these transitions, we performed frontier orbital analyses. Figure 4 depicts the HOMOs and LUMOs of **1′**−**3′**. As expected from the high contribution of Au (6sp) atomic orbitals to the frontier orbitals (>50%) (Figure 3(ii)), both HOMOs and LUMOs were found predominantly around the gold atoms in all the clusters. Among the three

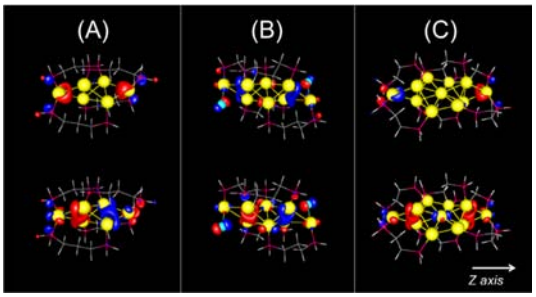

Figure 4. LUMOs (top) and HOMOs (bottom) of (A) $[Au_6(H_2P(CH_2)_3PH_2)_4]^{2+}$ (**1′**), (B) $[Au_8(H_2P(CH_2)_3PH_2)_4Cl_2]^{2+}$ (**2′**), and (C) $[Au_{11}(H_2P(CH_2)_2PH_2)_6]^{3+}$ (**3′**). The *z*-axis was chosen along the longitudinal direction of the gold core.

dx.doi.org/10.1021/ic4005592 | *Inorg. Chem.* 2013, 52, 6570−6575

clusters, the all-phosphine types **1′** and **3′** showed similar profiles. The LUMOs were found near the *exo* gold atoms, whereas the HOMOs were located on the shared edges of the polyhedral core (tetrahedral Au_4 for **1′** and toroidal Au_9 for **3′**) and Au_3 triangles. Thus, core → *exo* intermetal transition processes are likely responsible for the intense visible absorption bands seen in the spectra (Figure 3(iii)). The similarity between **1′** and **3′** in the orbital distribution pattern allowed to account for the transition energy difference based on a simple fusion model. As shown in Figure 5, the Au_{11} cluster

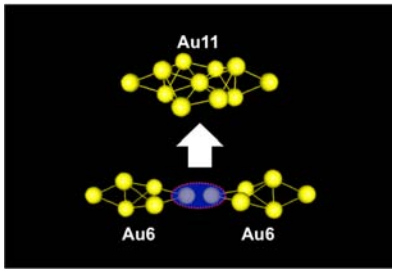

Figure 5. Schematic illustration of the generation of [core+*exo*]-type Au_{11} cluster through the fusion of two Au_6 units of **1** by sharing an *exo* atom.

unit could be constructed by the fusion of two Au_6 units of **1** by sharing an *exo* atom. Simple mixing of MOs of two Au_6 clusters would result in a decrease in the HOMO−LUMO gap, which is consistent with the lower excitation energy of the Au_{11} cluster (**3**).

On the other hand, the orbital distribution pattern of **2′** with the anionic chloride ligands was obviously different. The HOMO and LUMO were both located mainly near the shared edges, with the former being inside the core and the latter outside the core, respectively (Figure 4B). Remarkably, the LUMO density on the *exo* gold atoms was much sparser than on those of **1′** and **3′**, which may be related to the low oscillator strength of **2′** (Table 3) and also the low ε value of **2** (Table 1) in the first excitation transitions. The different HOMO/LUMO distribution profile of **2′** can be correlated with the relatively greater distance of the *exo* atoms from the bitetrahedral core in **2**. The enhancement of the Au(I) character of the *exo* gold atoms by the bonded Cl ligands may also contribute, but it does not seem to be a major factor, considering the comparable charges on the *exo* gold atoms in all three clusters (Table 2). Thus subtle geometric differences likely affected the HOMO/LUMO distribution patterns.

Nevertheless, the three clusters exhibited a similar directionality in their lowest-energy electronic transitions. Thus, all the first excitations occurred in the core (HOMO) → *exo* (LUMO) direction. Accordingly, clear contributions from the p orbitals of *exo* gold atoms and/or gold atoms on the shared edges were found along the *z*-axis in Figure 4. In this connection, it has been suggested that symmetry breaking in the icosahedral Au_{13} core through vertex-shared dimerization causes the generation of a lower-energy band in biicosahedral Au_{25} clusters.[39] Likewise, here the attachment of *exo* gold atoms to the polyhedral cores induced symmetry breaking in the cores, allowing the emergence of unique absorption bands with lower transition energies.

CONCLUSIONS

Unlike conventional colloidal metal clusters, ultrasmall gold clusters in the subnanometer regime exhibit molecule-like behaviors. Among them, the present [core+*exo*]-type gold clusters are exceptional in showing an unusual isolated absorption band in the visible region. Through systematic studies on these three crystallographically characterized clusters of different nuclearity, we have shown that not only the nuclearity but also the cluster geometry governs their optical properties and that there was no correlation between first excitation energy and nuclearity for the [core+*exo*]-type clusters. Theoretical studies indicated that these clusters had similar electronic structures, with the *exo* gold atoms critically involved in the generation of the HOMO and LUMO bands responsible for the appearance of the experimentally observed visible absorptions. Together with the crystallographic structural information, it was suggested that subtle geometric differences significantly affected HOMO/LUMO distribution patterns and optical properties. Overall we have found that, as a general trend, simple attachment of extra gold atom(s) on the surface of conventional metallic cores leads to the emergence of entirely distinct electronic structures. Rational design based on this principle would be useful for the exploration of novel metal cluster- or nanoparticle-based entities with unique functions.

EXPERIMENTAL SECTION

Optical absorption spectra were recorded on a JASCO V-670 double-beam spectrometer with a quartz cell of a 1-cm path length at 25 °C. Dichloromethane, methanol, and acetonitrile (spectroscopic grade) were purchased from Kanto Chemical and used as received. Crystals of **1**−**3**, which were prepared and identified as reported previously,[27−29] were weighed (∼3 mg) and dissolved in the designated solvents, and the resulting solutions were subjected to the spectral analyses. The purity and retention of the original cluster composition in solution were checked by ESI-MS spectra (Bruker micrOTOF) of the samples used for the absorption spectral measurements.

COMPUTATIONAL METHODS

All the calculations have been performed at density functional theory (DFT) level with the TURBOMOLE package.[40] Geometry optimizations and vibrational frequency analyses have been computed at BP86[41,42]/ double-ς plus polarization (def-SVP)[43] level. The resolution of the identity (RI) approximation of the coulomb interaction[44] was used for speeding up calculations. Single-point ground-state calculations were performed at the B3LYP level[45,46] with basis sets of triple-ς valence plus polarization quality (def2-TZVP; for Au) and split valence plus polarization quality (def2-SVP; for the other elements).[47] The same exchange-correlation functional and basis sets were adopted for the subsequent calculations of electronic excitation spectra using the TD-DFT method. In all calculations, default 60-electron relativistic effective core potentials (ECPs)[48] were employed for the Au atom.

Crystallographically determined geometric structures of gold clusters[27−29] after replacement of phenyl groups with hydrogen atoms were used for initial structures of geometry optimization calculations. The fully optimized structures, which were checked to be local minima by frequency calculations, adopted the D_2 (**1′**), C_i (**2′**), and C_2 (**3′**) symmetry point groups, respectively. The ground and excited state calculations of **1′**−**3′** were performed considering the symmetries. Unconstrained optimizations were also performed to check that the symmetry constraints did not introduce any inconsistencies.

dx.doi.org/10.1021/ic4005592 | *Inorg. Chem.* 2013, 52, 6570−6575

■ ASSOCIATED CONTENT

Supporting Information

Absorption spectra of $\mathbf{1}\cdot(NO_3)_2$, $\mathbf{2}\cdot(PF_6)_2$, and $\mathbf{3}\cdot(SbF_6)_3$ in methanol, acetonitrile, and dichloromethane, $\mathbf{2}\cdot(SbF_6)_2$ in dichloromethane, and $\mathbf{2}\cdot Cl_2$ in acetonitrile. This material is available free of charge via the Internet at http://pubs.acs.org.

■ AUTHOR INFORMATION

Corresponding Author

*E-mail: konishi@ees.hokudai.ac.jp.

Notes

The authors declare no competing financial interest.

■ ACKNOWLEDGMENTS

This work was partially supported by the MEXT/JSPS Grant-in-Aids (20111009 (Innovative Areas "Emergence in Chemistry") for K.K. and 24750001 for Y.S.), the Asahi Glass Foundation (K.K.), the Sasakawa Scientific Research Grant and Tanaka Precious Metals Group (Y.S.). We also thank Japan Science and Technology Agency (JST), Core Research for Evolutional Science and Technology (CREST) and Advanced Low Carbon Technology Research and Development Program (ALCA) for K.K. The help of Mr. Y. Kamei in spectral measurements is also acknowledged.

■ REFERENCES

(1) Sardar, R.; Funston, A. M.; Mulvaney, P.; Murray, R. W. *Langmuir* **2009**, *25*, 13840−13851.
(2) Jin, R. *Nanoscale* **2010**, *2*, 343−362.
(3) Tsukuda, T. *Bull. Chem. Soc. Jpn.* **2012**, *85*, 151−168.
(4) Lu, Y.; Chen, W. *Chem. Soc. Rev.* **2012**, *41*, 3594−3623.
(5) Mirkin, C. A.; Letsinger, R. L.; Mucic, R. C.; Storhoff, J. J. *Nature* **1996**, *382*, 607−609.
(6) De, M.; Ghosh, P. S.; Rotello, V. M. *Adv. Mater.* **2008**, *20*, 4225−4241.
(7) Alvarez, M. M.; Khoury, J. T.; Schaaff, T. G.; Shafigullin, M. N.; Vezmar, I.; Whetten, R. L. *J. Phys. Chem. B* **1997**, *101*, 3706−3712.
(8) Chen, S. W.; Ingram, R. S.; Hostetler, M. J.; Pietron, J. J.; Murray, R. W.; Schaaff, T. G.; Khoury, J. T.; Alvarez, M. M.; Whetten, R. L. *Science* **1998**, *280*, 2098−2101.
(9) Negishi, Y.; Nobusada, K.; Tsukuda, T. *J. Am. Chem. Soc.* **2005**, *127*, 5261−5270.
(10) Zheng, J.; Zhang, C. W.; Dickson, R. M. *Phys. Rev. Lett.* **2004**, *93*, 0774021−0774024.
(11) Udaya Bhaskara Rao, T.; Pradeep, T. *Angew. Chem., Int. Ed.* **2010**, *49*, 3925−3929.
(12) Kawasaki, H.; Hamaguchi, K.; Osaka, I.; Arakawa, R. *Adv. Funct. Mater.* **2011**, *21*, 3508−3515.
(13) Sharma, J.; Yeh, H.-C.; Yoo, H.; Werner, J. H.; Martinez, J. S. *Chem. Commun.* **2010**, *46*, 3280−3282.
(14) Chen, W.-T.; Hsu, Y.-J.; Kamat, P. V. *J. Phys. Chem. Lett.* **2012**, *3*, 2493−2499.
(15) Hall, K. P.; Mingos, D. M. P. *Prog. Inorg. Chem.* **1984**, *32*, 237−325.
(16) Fernández, E. J.; Monge, M. In *Modern Supramolecular Gold Chemistry*; Laguna, A., Ed.; Wiley-VCH: Weinheim, Germany, 2008; pp 131−179.
(17) Schmid, G. *Angew. Chem., Int. Ed.* **2008**, *47*, 3496−3498.
(18) Briant, C. E.; Hall, K. P.; Mingos, D. M. P.; Wheeler, A. C. *J. Chem. Soc., Dalton Trans.* **1986**, 687−692.
(19) van der Velden, J. W. A.; Beurskens, P. T.; Bour, J. J.; Bosman, W. P.; Noordik, J. H.; Kolenbrander, M.; Buskes, J. A. K. M. *Inorg. Chem.* **1984**, *23*, 146−151.
(20) Vollenbroek, F. A.; Bosman, W. P.; Bour, J. J.; Noordik, J. H.; Beurskens, P. T. *J. Chem. Soc., Chem. Commun.* **1979**, 387−388.
(21) Wen, F.; Englert, U.; Gutrath, B.; Simon, U. *Eur. J. Inorg. Chem.* **2008**, 106−111.
(22) Copley, R. C. B.; Mingos, D. M. P. *J. Chem. Soc., Dalton Trans.* **1996**, 479−489.
(23) Smits, J. M. M.; Bour, J. J.; Vollenbroek, F. A.; Beurskens, P. T. *J. Crystallogr. Spectrosc. Res.* **1983**, *13*, 355−363.
(24) Nunokawa, K.; Onaka, S.; Yamaguchi, T.; Ito, T.; Watase, S.; Nakamoto, M. *Bull. Chem. Soc. Jpn.* **2003**, *76*, 1601−1602.
(25) Briant, C. E.; Theobald, B. R. C.; White, J. W.; Bell, L. K.; Mingos, D. M. P. *J. Chem. Soc., Chem. Commun.* **1981**, 201−202.
(26) Shichibu, Y.; Konishi, K. *Small* **2010**, *6*, 1216−1220.
(27) van der Velden, J. W. A.; Bour, J. J.; Steggerda, J. J.; Beurskens, P. T.; Roseboom, M.; Noordik, J. H. *Inorg. Chem.* **1982**, *21*, 4321−4324.
(28) Kamei, Y.; Shichibu, Y.; Konishi, K. *Angew. Chem., Int. Ed.* **2011**, *50*, 7442−7445.
(29) Shichibu, Y.; Kamei, Y.; Konishi, K. *Chem. Commun.* **2012**, *48*, 7559−7561.
(30) Jadzinsky, P. D.; Calero, G.; Ackerson, C. J.; Bushnell, D. A.; Kornberg, R. D. *Science* **2007**, *318*, 430−433.
(31) Heaven, M. W.; Dass, A.; White, P. S.; Holt, K. M.; Murray, R. W. *J. Am. Chem. Soc.* **2008**, *130*, 3754−3755.
(32) Zhu, M.; Aikens, C. M.; Hollander, F. J.; Schatz, G. C.; Jin, R. *J. Am. Chem. Soc.* **2008**, *130*, 5883−5885.
(33) Pyykkö, P. *Angew. Chem., Int. Ed.* **2004**, *43*, 4412−4456.
(34) Walter, M.; Akola, J.; Lopez-Acevedo, O.; Jadzinsky, P. D.; Calero, G.; Ackerson, C. J.; Whetten, R. L.; Grönbeck, H.; Häkkinen, H. *Proc. Natl. Acad. Sci. U.S.A.* **2008**, *105*, 9157−9162.
(35) Pei, Y.; Gao, Y.; Shao, N.; Zeng, X. C. *J. Am. Chem. Soc.* **2009**, *131*, 13619−13621.
(36) Ivanov, S. A.; Arachchige, I.; Aikens, C. M. *J. Phys. Chem. A* **2011**, *115*, 8017−8031.
(37) Mingos, D. M. P.; Slee, T.; Zhenyang, L. *Chem. Rev.* **1990**, *90*, 383−402.
(38) Zhang, H. F.; Stender, M.; Zhang, R.; Wang, C.; Li, J.; Wang, L. S. *J. Phys. Chem. B* **2004**, *108*, 12259−12263.
(39) Nobusada, K.; Iwasa, T. *J. Phys. Chem. C* **2007**, *111*, 14279−14282.
(40) TURBOMOLE V6.3 2011, a development of University of Karlsruhe and Forschungszentrum Karlsruhe GmbH, 1989−2007, TURBOMOLE GmbH, since 2007; available from http://www.turbomole.com
(41) Becke, A. D. *Phys. Rev. A* **1988**, *38*, 3098−3100.
(42) Perdew, J. P. *Phys. Rev. B* **1986**, *33*, 8822−8824.
(43) Schäfer, A.; Horn, H.; Ahlrichs, R. *J. Chem. Phys.* **1992**, *97*, 2571−2577.
(44) Ahlrichs, R.; Bar, M.; Haser, M.; Horn, H.; Kolmel, C. *Chem. Phys. Lett.* **1989**, *162*, 165−169.
(45) Lee, C. T.; Yang, W. T.; Parr, R. G. *Phys. Rev. B* **1988**, *37*, 785−789.
(46) Becke, A. D. *J. Chem. Phys.* **1993**, *98*, 5648−5652.
(47) Weigend, F.; Ahlrichs, R. *Phys. Chem. Chem. Phys.* **2005**, *7*, 3297−3305.
(48) Andrae, D.; Häussermann, U.; Dolg, M.; Stoll, H.; Preuss, H. *Theor. Chim. Acta* **1990**, *77*, 123−141.